

Growth and transport properties of topological insulator Bi_2Se_3 thin film on a ferromagnetic insulating substrate

Shanna Zhu(朱珊娜), Gang Shi(史刚), Peng Zhao(赵鹏), Dechao Meng(孟德超), Genhao Liang(梁根豪), Xiaofang Zhai(翟晓芳), Yalin Lu(陆亚林), Yongqing Li(李永庆), Lan Chen(陈岚), Kehui Wu(吴克辉)

Citation: Chin. Phys. B . 2018, 27(7): 076801. **doi:** 10.1088/1674-1056/27/7/076801

Journal homepage: http://cpb.iphy.ac.cn; http://iopscience.iop.org/cpb

What follows is a list of articles you may be interested in

Segregations and desorptions of Ge atoms in nanocomposite $Si_{1-x}Ge_x$ films during high-temperature annealing

Yu Wang(汪煜), Meng Yang(杨濛), Gang Wang(王刚), Xiao-Xu Wei(魏晓旭), Jun-Zhuan Wang(王军转), Yun Li(李昀), Ze-Wen Zou(左则文), You-Dou Zheng(郑有炓), Yi Shi(施毅)

Chin. Phys. B . 2017, 26(12): 126801. **doi:** 10.1088/1674-1056/26/12/126801

Structural characteristics of surface-functionalized nitrogen-doped diamond-like carbon films and effective adjustment to cell attachment

Liu Ai-Ping, Liu Min, Yu Jian-Can, Qian Guo-Dong, Tang Wei-Hua

Chin. Phys. B . 2015, 24(5): 056804. **doi:** 10.1088/1674-1056/24/5/056804

Characterization of tetragonal distortion in a thick $Al_{0.2}Ga_{0.8}N$ epilayer with an AlN interlayer by Rutherford backscattering/channeling

Wang Huan, Yao Shu-De

Chin. Phys. B . 2014, 23(9): 096801. **doi:** 10.1088/1674-1056/23/9/096801

Two crucial factors influencing quality of GaAs on Ge substrate

Deng Chuang, Men Chuan-Ling, Chen Da

Chin. Phys. B . 2014, 23(4): 046805. **doi:** 10.1088/1674-1056/23/4/046805

Molecular beam epitaxy and superconductivity of stoichiometric FeSe and $K_xFe_{2-y}Se_2$ crystalline films

Wang Li-Li, Ma Xu-Cun, Chen Xi, Xue Qi-Kun

Chin. Phys. B . 2013, 22(8): 086801. **doi:** 10.1088/1674-1056/22/8/086801

Growth and transport properties of topological insulator Bi_2Se_3 thin film on a ferromagnetic insulating substrate*

Shanna Zhu(朱珊娜)[1,2], Gang Shi(史刚)[1,2], Peng Zhao(赵鹏)[1,2], Dechao Meng(孟德超)[3,4], Genhao Liang(梁根豪)[3], Xiaofang Zhai(翟晓芳)[3,5], Yalin Lu(陆亚林)[3,5,6], Yongqing Li(李永庆)[1], Lan Chen(陈岚)[1,2,†], and Kehui Wu(吴克辉)[1,2,7,‡]

[1] *Beijing National Laboratory for Condensed Matter Physics, Institute of Physics, Chinese Academy of Sciences, Beijing* 100190, *China*
[2] *School of Physical Sciences, University of Chinese Academy of Sciences, Beijing* 100049, *China*
[3] *Hefei National Laboratory for Physical Sciences at the Microscale, University of Science and Technology of China, Hefei* 230026, *China*
[4] *Microsystem and Terahertz Research Center & Institute of Electronic Engineering, CAEP, Mianyang* 621900, *China*
[5] *Synergy Innovation Center of Quantum Information and Quantum Physics, University of Science and Technology of China, Hefei* 230026, *China*
[6] *National Synchrotron Radiation Laboratory, University of Science and Technology of China, Hefei* 230026, *China*
[7] *Collaborative Innovation Center of Quantum Matter, Beijing* 100871, *China*

(Received 12 April 2018; revised manuscript received 4 May 2018; published online 25 June 2018)

Exchange coupling between topological insulator and ferromagnetic insulator through proximity effect is strongly attractive for both fundamental physics and technological applications. Here we report a comprehensive investigation on the growth behaviors of prototype topological insulator Bi_2Se_3 thin film on a single-crystalline $LaCoO_3$ thin film on $SrTiO_3$ substrate, which is a strain-induced ferromagnetic insulator. Different from the growth on other substrates, the Bi_2Se_3 films with highest quality on $LaCoO_3$ favor a relatively low substrate temperature during growth. As a result, an inverse dependence of carrier mobility with the substrate temperature is found. Moreover, the magnetoresistance and coherence length of weak antilocalization also have a similar inverse dependence with the substrate temperature, as revealed by the magnetotransport measurements. Our experiments elucidate the special behaviors in $Bi_2Se_3/LaCoO_3$ heterostructures, which provide a good platform for exploring related novel quantum phenomena, and are inspiring for device applications.

Keywords: topological insulator, ferromagnetic insulator, molecular beam epitaxy, magnetotransport properties

PACS: 68.55.–a, 73.50.–h, 75.47.–m, 81.15.–z **DOI:** 10.1088/1674-1056/27/7/076801

1. Introduction

The discovery of three-dimensional (3D) topological insulators (TIs) has attracted much attention in recent years due to their rich physics and promising applications in electronic and spintronic devices.[1–9] The exotic gapless surface states of TIs are protected by time-reversal symmetry (TRS), with locked spin-momentum which is immune to backscattering. On the other hand, the breaking of TRS will open up a gap in the Dirac surface states of TIs, leading to a massive Dirac fermion state which can give rise to many novel phenomena.[10–15] Introducing ferromagnetism into TIs through proximity effect with a ferromagnetic insulator (FMI) is an effective way to break the TRS, and it avoids bringing extra impurities compared with doping method.[16–27]

The prototype topological insulator, Bi_2Se_3, is a layered material with relatively large bulk energy gap among 3D TIs.[3,4] Experiments on the growth of Bi_2Se_3 thin films on different kinds of substrates have been reported, including Si(111), GaAs(111), graphene, $SrTiO_3$(111), Al_2O_3(0001), and so on.[28–33] However, experiments on insulating ferromagnetic substrates are limited to a few kinds of materials, since the existing FMIs are very scarce in nature.[34] So far, the commonly used FMIs mostly possess low-symmetry structures associated with a poor growth quality, and the few known high-symmetry materials either have very low Curie temperatures ($\leq$ 17 K), or require chemical doping of an otherwise antiferromagnetic matrix.[35]

$LaCoO_3$ (LCO) single-crystalline thin film under tensile strain is a newly reported high-temperature perovskite ferromagnetic insulator.[35–38] The tensile-strained $LaCoO_3$ film is shown to be a rare undoped high-symmetry FMI with a remarkably high T_C of up to 85 K. Both experiments and first-principles calculations demonstrate tensile-strain-induced ferromagnetism due to the spin-state transition of Co^{3+} ion, which does not exist in bulk $LaCoO_3$. More importantly, the strained $LaCoO_3$ thin film can be prepared epitaxially on substrate such as the $SrTiO_3$ (STO) with an atomically flat surface,[35] which is crucial for growing high-quality Bi_2Se_3

*Project supported by the National Key R&D Program of China (Grant Nos. 2016YFA0300904 and 2016YFA0202301), the National Natural Science Foundation of China (Grant Nos. 11334011, 11674366, 11674368, and 11761141013), and the Strategic Priority Research Program of the Chinese Academy of Sciences (Grant Nos. XDB07010200 and XDPB06).

†Corresponding author. E-mail: lchen@iphy.ac.cn
‡Corresponding author. E-mail: khwu@iphy.ac.cn

© 2018 Chinese Physical Society and IOP Publishing Ltd

thin films onto it. Recently, we have found ferromagnetism in the Bi_2Se_3 film grown on $LaCoO_3/SrTiO_3$ by the proximity effect, implying that this system would be a promising platform for studying novel transport phenomena in TI/ferromagnetic structures.[39]

In this work, we systematically studied the growth behaviors of topological insulator Bi_2Se_3 thin films on $LaCoO_3/SrTiO_3$ by molecular beam epitaxy (MBE). We find that the optimal condition for Bi_2Se_3 to grow on LCO/STO is at a much lower substrate temperature, around 150 °C, as compared with the optimal temperature on bare STO. The thus obtained Bi_2Se_3 thin films display a well-organized morphology and high carrier mobility, similar to those grown on bare STO substrates at higher temperature. While at higher growth temperatures, Bi_2Se_3 films on LCO exhibit disordered film morphology and decreased carrier mobility. The magnetoresistance and characteristic weak antilocalization effect are also reduced at higher growth temperatures. These unusual behaviors may be attributed to the subtle strain stress and large thermal-expansion coefficient of LCO. Our exploration and realization of the Bi_2Se_3/LCO heterostructure will be promising for developing versatile spintronic device applications.

2. Experimental methods

2.1. Sample growth

The growth of Bi_2Se_3 thin films was carried out by a home-made MBE system in an ultrahigh vacuum (UHV) chamber with a base pressure lower than 2.0×10^{-10} Torr, equipped with reflection high-energy electron diffraction (RHEED) facility. As-prepared LCO single-crystalline thin films on (001)-oriented STO substrates were transferred into the UHV chamber and were degassed at 300 °C for about one hour before growth. High-purity Bi (99.997%) and Se (99.999%) sources were co-evaporated from the standard Knudsen cells, and deposited onto the surface of LCO, which was kept at a certain temperature during growth. The fluxes of Bi and Se were calibrated by a quartz crystal microbalance thickness monitor, and a high Se/Bi flux ratio of 10/1 was used in order to reduce the amount of Se vacancies. The typical growth rate of Bi_2Se_3 thin films used in this work was about 0.3 nm per minute. In-situ real-time RHEED was performed to monitor the growth dynamics during the whole process. For comparison, Bi_2Se_3 films were also grown on as-treated bare STO (001) substrates with the same procedures as that on LCO/STO.

2.2. Characterization

In-situ RHEED patterns were recorded during the film growth process to identify the film quality. Crystal structures of films were measured by x-ray diffraction (XRD) using a single crystal x-ray diffractometer (PANalytical) with Cu $K_{\alpha 1}$ radiation of wavelength 1.5406 Å in the ω–2θ scan. The surface morphologies of Bi_2Se_3 films were characterized by an atomic force microscope (AFM) in tapping mode.

Low-temperature electrical transport measurements were conducted in a helium cryostat system where a superconducting magnet was equipped, with temperature down to ~ 1.7 K and magnetic field up to ± 9 T. The Bi_2Se_3 films on LCO/STO were patterned into Hall bar geometry with a channel width of about 500 μm. The applied current was along the channel (denoted by x axis) and magnetic field applied in the perpendicular direction (z axis). Several batches of samples grown at different conditions were tested, and the typical results will be shown below. We also carried out transport measurements of the Bi_2Se_3 films grown on STO, to provide a reference data on non-magnetic substrates.

3. Results and discussion

Figure 1 shows the evolution of RHEED patterns of Bi_2Se_3 film on LCO/STO substrate during growth. Before the growth of Bi_2Se_3 film, straight stripes of RHEED pattern shown in Fig. 1(a) were observed, reflecting a clean and flat surface of the $LaCoO_3$ film. When the Bi_2Se_3 film started to grow, the original stripes disappeared, and a new characteristic pattern corresponding to Bi_2Se_3 occurred, as shown in Fig. 1(b). After the growth of 2–3 quintuple-layers (QLs) of Bi_2Se_3, the streaky RHEED pattern becomes clear, indicating a crystalline film forming. As the film grew thicker, the stripes in RHEED pattern became bright and sharp accordingly, as illustrated in Figs. 1(c) and 1(d). The clear and sharp stripes indicate highly crystalline and smooth surface of Bi_2Se_3 film. Besides, QL-by-QL growth mode is determined by a periodic oscillation of diffraction intensity in RHEED pattern during film growth.

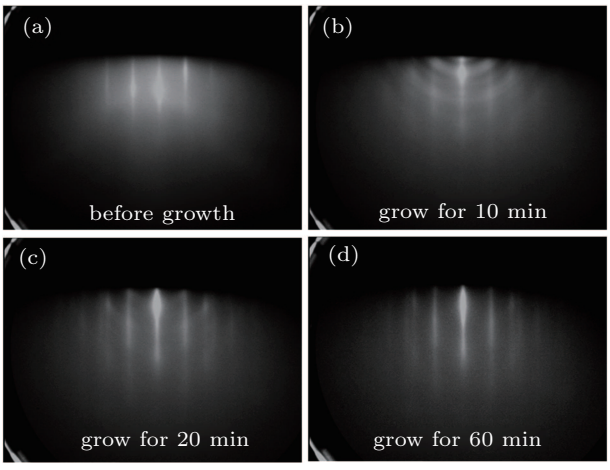


Fig. 1. RHEED patterns recorded during the deposition of Bi_2Se_3 film on $LaCoO_3$ substrate. (a) The surface of $LaCoO_3$ thin film after degassing, and before the Bi_2Se_3 film growth. (b), (c), and (d) were taken when the Bi_2Se_3 film has grown for 10 min (3 QL), 20 min (6 QL), and 60 min (18 QL), respectively.

High quality of the Bi_2Se_3 film is also verified by XRD measurement on Bi_2Se_3/LCO samples. In Fig. 2, the Bi_2Se_3 film exhibits $(00l)$ ($l = 3n$, where n is an integer) type of reflections over the 10°–80° scan range without other set of peaks of bulk Bi_2Se_3, indicating that the film is of single crystalline quality along the growth direction. The Bragg peak positions of Bi_2Se_3 film grown on LCO/STO(001) agree very well with the reference data of ICSD standard card for Bi_2Se_3 single crystal, suggesting that the film is in good relaxation and the lattice parameter is consistent with its bulk value. In addition, all films grown on LCO within a range of different conditions show similar features in XRD patterns, indicating that single crystalline phase of Bi_2Se_3 can be obtained among these samples.

To investigate the influence of different substrate temperatures during growth on the film morphology, we scanned the surface of the Bi_2Se_3 films through AFM technique. Figure 3 shows the AFM images of Bi_2Se_3 films grown on LCO/STO substrates with different substrate temperatures ranged from 130 °C to over 300 °C during growth. Comparing the images shown in Figs. 3(a)–3(h), we find that the optimal morphology is obtained at a substrate temperature of 150 °C (Fig. 3(b)), which displays the characteristic pyramid-shaped layered structure in good order. At a substrate temperature as low as 130 °C, the film is not well crystallized (shown in Fig. 3(a)) due to insufficient diffusion of Bi and Se atoms. While at a substrate temperature higher than 150 °C, the pyramid-shaped islands on the surface of the film become distorted gradually, and the disorder in morphology becomes more visible at higher temperatures above 200 °C. The high temperature may influence the underlying stain stress from LCO substrate, and the underneath Bi_2Se_3 layers seem to become inflated and coarse, indicating it is unfavorable for the Bi_2Se_3 film to grow at such high substrate temperature. When the substrate is heated to over 300 °C, the film will decompose because the Se atoms are desorbed from the substrate. In addition, at a larger scale, the integral morphology of Bi_2Se_3 film grown at 150 °C is also well-organized and uniformly distributed, with a small root-mean-square roughness of 1.36 nm.

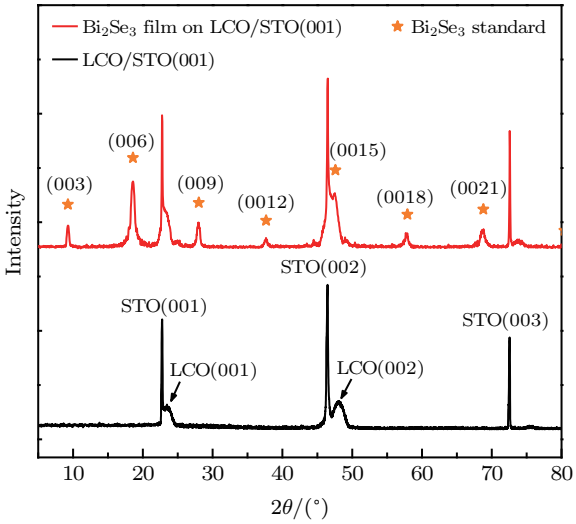


Fig. 2. X-ray diffraction spectrum of a 20 QL Bi_2Se_3 film on $LaCoO_3/SrTiO_3(001)$ (red line) and the data of an as-prepared $LaCoO_3$ film on $SrTiO_3(001)$ substrate (black line) for comparison. The standard data (ICSD card) of Bi_2Se_3 single crystal is also shown (marked as orange star symbols) as a reference.

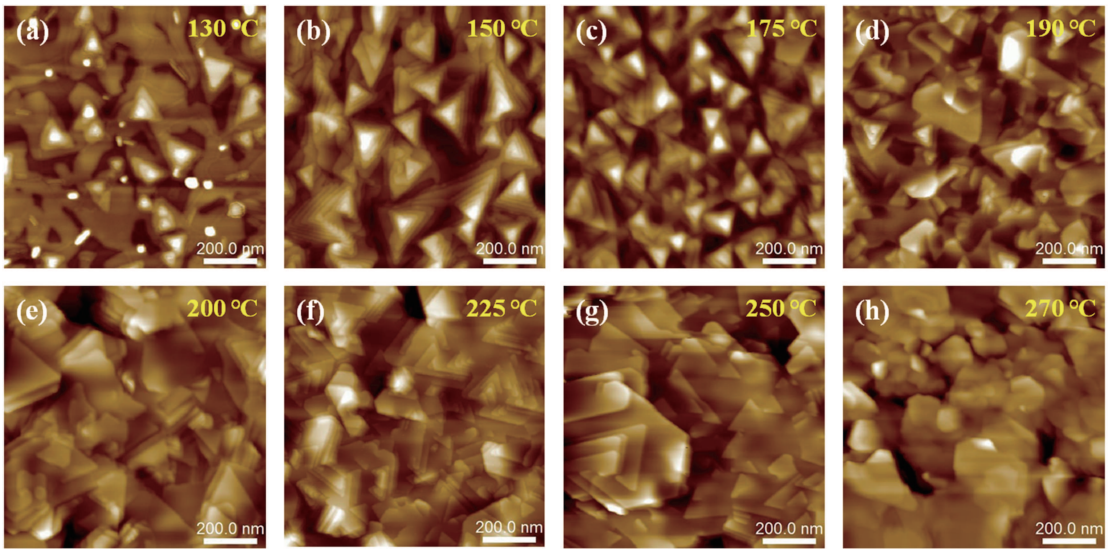


Fig. 3. AFM images (size: 1 μm×1 μm) of a series of Bi_2Se_3 films grown on $LaCoO_3/SrTiO_3(001)$ substrate at different substrate temperatures: (a) 130 °C, (b) 150 °C, (c) 175 °C, (d) 190 °C, (e) 200 °C, (f) 225 °C, (g) 250 °C, and (h) 270 °C. All the films have been grown for 60 min.

For comparison, the morphologies of Bi_2Se_3 films on pure STO(001) substrates were investigated under the same growth conditions. As shown in Fig. 4(a), at a substrate temperature of 150 °C, Bi_2Se_3 film on STO exhibits almost the same morphology as that in Fig. 3(b). While at higher temperatures (see Figs. 4(b)–4(d)), Bi_2Se_3 films on STO display a better morphology with increased triangle island size and larger terrace area, and each QL on the surface is clearly re-

solved, indicating the overall surface is much flatter. The significant difference between samples grown on LCO and pure STO implies that higher substrate temperature is not suitable for Bi_2Se_3 film growing on LCO, and the most favorable temperature is about 150 °C, much lower than that on STO substrate alone.

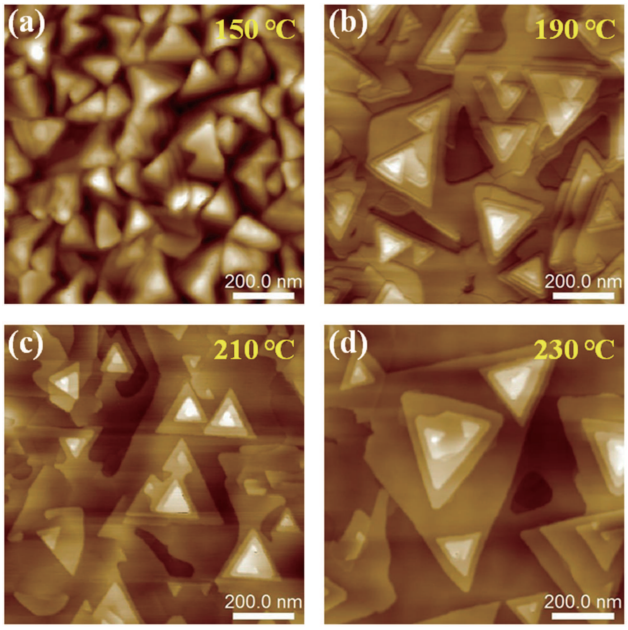


Fig. 4. AFM images (size: 1 μm×1 μm) of Bi_2Se_3 film grown on $SrTiO_3$(001) substrate at different substrate temperatures: (a) 150 °C, (b) 190 °C, (c) 210 °C, and (d) 230 °C. All the films have been grown for 60 min, under the same conditions as that in Fig. 3.

In general, Bi_2Se_3 thin films can be layer-by-layer grown on different kinds of substrates with even slight lattice mismatch, due to the van der Waals epitaxy. In these cases, including on the pure STO(001) substrate, Bi_2Se_3 thin film tends to have a smoother surface at a relatively higher temperature above 200 °C, which allows sufficient diffusion of the Bi and Se atoms.[30–33] While in the case of LCO/STO, higher substrate temperature seems to have a negative influence on the film quality of Bi_2Se_3. Compared with other substrates, LCO has a larger thermal-expansion coefficient.[36] The expanded lattice of underlying LCO layer and the accompanied influence on strain stress due to lattice mismatch becomes more obvious at high substrate temperature, which results in the disordered morphology of films. Therefore, by exploring a wide range of possible growth temperatures, we find that only at the relatively lower temperature can Bi_2Se_3 film be grown onto LCO/STO in free-standing QL-by-QL mode, as it does on other substrates.

For transport measurements, we chose a thickness of 20 QL for the Bi_2Se_3 films, which is well above the thickness threshold of 6 nm. Below this threshold, the top and bottom surface of Bi_2Se_3 may be coupled by quantum tunneling and lead to a hybridization gap near Dirac point, similar to the result brought by strong magnetic interaction.[40] In Fig. 5(a), we plot the Hall resistance (R_{xy}) of Bi_2Se_3/LCO samples grown at different substrate temperatures measured in the perpendicular applied magnetic field at 1.7 K. For all the samples, the Hall resistance has a nearly linear dependence on the magnetic field, suggesting that one type of carriers dominate the transport. Using the one-band model, we can obtain that the carriers in all the Bi_2Se_3 films are n type, and the initial carrier densities are in the range of 2.5×10^{13}–3.5×10^{13} cm^{-2}, which are consistent with the results for Bi_2Se_3/STO samples.[41,42]

The initial carrier density and carrier mobility of four Bi_2Se_3/LCO samples grown at different substrate temperatures (T_{sub}) are plotted in Fig. 5(b). The sample with best morphology that grown at optimal T_{sub} = 150 °C has a carrier density 2.7×10^{13} cm^{-2} and mobility 659 $cm^2\cdot V^{-1}\cdot s^{-1}$. Such carrier mobility is as high as that of Bi_2Se_3/STO control samples,[43] indicating high film quality with pristine good transport properties is achieved at the optimal growth condition. On the other hand, the carrier density of the film increases gradually when T_{sub} goes up, probably due to the increasing density of Se vacancies at higher substrate temperature. This behavior for Bi_2Se_3 films grown on ferromagnetic LCO/STO is the same as that on non-magnetic STO substrates. However, unlike the usual case on other substrates, the carrier mobility of the film decreases when T_{sub} goes up, implying more scattering and disorder inside the film. This may be ascribed to the lattice distortion due to the expanded lattice of LCO and defects such as the dislocations arisen at higher substrate temperatures, just as inferred from the film morphology.

Figure 5(c) shows the magnetoresistance (MR) of Bi_2Se_3/LCO samples grown at different T_{sub}, together with a Bi_2Se_3/STO control sample measured at 1.7 K under a perpendicular magnetic field. The MR, defined as $MR = [\rho_{xx}(H)-\rho_{xx}(0)]/\rho_{xx}(0)$, where $\rho_{xx}(H)$ is the longitudinal resistivity as a function of the magnetic field H, is positive for all curves measured here. In the range near zero field, MR is characterized by the cusp-like shape due to the weak antilocalization (WAL) effect, which is a characteristic sign for strong spin-orbit coupled TI materials.[24,44,45] On the surface of TI materials, backscattering is prohibited due to time-reversal symmetry when the magnetic field is absent. With an increasing magnetic field, which breaks the time-reversal symmetry, backscattering starts to occur and leads to a rise in the MR.[45] The WAL effect is pronounced in the Bi_2Se_3/STO control sample. However, for the Bi_2Se_3/LCO samples, MR are reduced significantly, meaning that the WAL effect is suppressed due to the presence of underlying magnetic layer.[19,21] Moreover, with the increasing T_{sub}, MR decreases monotonously for the Bi_2Se_3/LCO samples, implying further suppression of the WAL effect. The further reduced MR is caused by extra scattering from lattice disorder in the film with higher T_{sub}, which becomes dominated near zero field and thus result in a relatively decreased MR in higher field. Besides, it should be noted that, for the non-magnetic Bi_2Se_3/STO samples, MR increases with raised T_{sub}, which is contrary to the behavior of Bi_2Se_3/LCO samples.

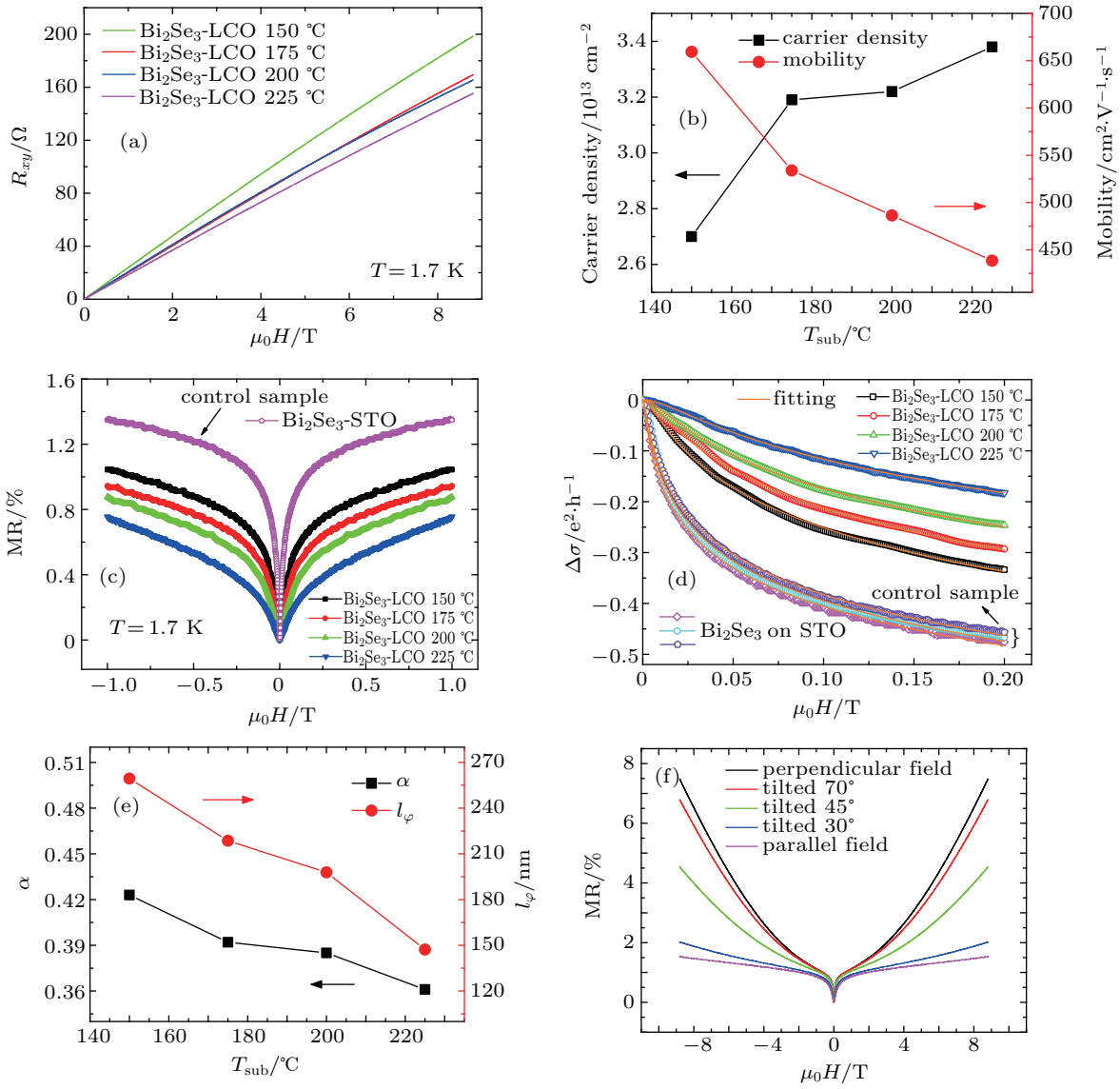


Fig. 5. Magnetotransport properties of the Bi_2Se_3/LCO heretostructure devices. All the data are measured at 1.7 K. (a) Hall resistance (R_{xy}) of several Bi_2Se_3/LCO samples as a function of the perpendicular magnetic field. (b) Initial carrier density (black squares) and carrier mobility (red circles) derived from several Bi_2Se_3/LCO samples grown at different substrate temperatures (denoted by T_{sub}) ranging from 150 °C to 225 °C. (c) Magnetoresistance (MR) measured in perpendicular magnetic field of four Bi_2Se_3/LCO samples (in solid symbols) grown at $T_{sub} = 150$ °C, 175 °C, 200 °C, 225 °C, respectively, and a control sample (in pink open symbol) of Bi_2Se_3/STO grown at $T_{sub} = 150$ °C. (d) Magnetoconductivity in low-field range of the corresponding samples in (c) as well as two additional curves of the Bi_2Se_3/STO control sample with $T_{sub} = 150$ °C at gate voltage 30 V and −100 V, respectively. The HLN fitting results of each curve are plotted in solid (orange) lines. (e) The fitting parameters of HLN equation for each Bi_2Se_3/LCO sample shown in (d). (f) MR of a typical Bi_2Se_3/LCO sample grown at optimal $T_{sub} = 150$ °C measured in tilted field. The tilted angle is defined as the angle between the applied magnetic field and the film plane.

Further analysis of the WAL effect is carried out by a quantitative fitting of low-field magnetoconductance (MC) data. The magnetoconductivity is defined as $\Delta\sigma(H) = \sigma_{xx}(H) - \sigma_{xx}(0)$, where the sheet conductance (σ) is calculated by the relation $\sigma_{xx} = \rho_{xx}/(\rho_{yx}^2 + \rho_{xx}^2)$. As proposed in the literature,[41–46] the WAL quantum corrections to the low-field magnetoconductivity in the strong spin–orbit coupling (SOC) limit can be described by the Hikami–Larkin–Nagaoka (HLN) equation[47]

$$\Delta\sigma(H) \cong -\alpha\frac{e^2}{2\pi^2\hbar}\left[\Psi\left(\frac{1}{2}+\frac{H_\varphi}{H}\right) - \ln\left(\frac{H_\varphi}{H}\right)\right],$$

where $\psi(x)$ is the digamma function, $H_\varphi = \frac{B_\varphi}{\mu_0} = \frac{1}{\mu_0}\frac{\hbar}{4el_\varphi^2}$ is the dephasing magnetic field, and l_φ is the phase coherence length. The coefficient $\alpha = 0.5$ is used for a system with single coherent channel, which is also expected for the electron transport on one surface of a 3D TI with a single Dirac cone.[41,42]

As plotted in Fig. 5(d), the magnetoconductivity of samples has an inverted shape as that in Fig. 5(c), and the fitting curves in orange lines agree very well with the experimental data. The reduced negative magnetoconductivity is an indicator of suppressed WAL effect in the magnetic samples. From the fitting data of HLN equation, we can obtain the two parameters α and l_φ, which are plotted in Fig. 5(e). For the Bi_2Se_3/LCO samples, both α and l_φ have an inverse

dependence on the T_{sub}. The smaller values of α and l_φ at higher T_{sub} suggests more scattering inside the films. While for the Bi_2Se_3/STO control sample, α takes a value very close to 0.5, consistent with the previous studies.[42,44] The coherence length l_φ has a larger value at higher T_{sub}, which is in contrast to the decreasing trend in Bi_2Se_3/LCO samples. The reduced coherence length and associated more scattering with increased T_{sub} further indicate a negative influence on the transport properties for Bi_2Se_3/LCO samples.

Transport properties in the tilted magnetic field are also measured for the Bi_2Se_3/LCO samples, as shown in Fig. 5(f). The MR has the largest value when it is measured in a perpendicular magnetic field, and is featured with a parabolic shape in higher field range, which is originated from the Lorentzian deflection of carriers.[44] When the applied field is tilted from the perpendicular direction to a smaller angle, the MR decreases, but maintains the similar shape. While when the field approaches the parallel direction, the MR decreases significantly, and it is no longer in the quadratic relationships with the magnetic field. In a parallel field, the WAL effect is manifested due to the absence of large parabolic background, which is similar to the results on STO substrates.[48]

The above data of magnetotransport measurements further indicate a crucial role played by the substrate temperature during growth, where the disorder arising from higher substrate temperature is proven to be disadvantageous for the transport properties of samples. These results are in consistence with the analysis of film morphology, and corroborate the conclusion that low substrate temperature is favorable for the growth of Bi_2Se_3/LCO.

4. Conclusion

In conclusion, we have performed a systematic investigation on the growth behaviors of epitaxial Bi_2Se_3 thin films on a ferromagnetic insulating LCO/STO substrate, which forms a new TI/FMI heterostructure. The Bi_2Se_3 films with highly crystalline structure and well-ordered surface are obtained at a relatively low substrate temperature of 150 °C during growth. Transport measurement confirms high carrier mobility in the sample grown at optimal conditions. An unusual dependence of film morphology and transport properties on the growth temperatures are observed, and can be attributed to the large thermal-expansion coefficient of LCO substrate and the increased strain stress at the interface at high substrate temperature. Our results and methodology of fabricating such high-quality TI/FMI heterostructure provide not only a platform for investigating the proximity-induced magnetism in TIs, but a versatile approach to explore the TI-based spintronic devices in applications.

References

[1] Hasan M Z and Kane C L 2010 *Rev. Mod. Phys.* **82** 3045
[2] Hsieh D, Qian D, Wray L, Xia Y, Hor Y S, Cava R J and Hasan M Z 2008 *Nature* **452** 970
[3] Zhang H J, Liu C X, Qi X L, Dai X, Fang Z and Zhang S C 2009 *Nat. Phys.* **5** 438
[4] Xia Y, Qian D, Hsieh D, Wray L, Pal A, Lin H, Bansil A, Grauer D, Hor Y S, Cava R J and Hasan M Z 2009 *Nat. Phys.* **5** 398
[5] Moore J E 2010 *Nature* **464** 194
[6] Fu L and Kane C L 2008 *Phys. Rev. Lett.* **100** 096407
[7] Vobornik I, Manju U, Fujii J, Borgatti F, Torelli P, Krizmancic D, Hor Y S, Cava R J and Panaccione G 2011 *Nano Lett.* **11** 4079
[8] Ferreira G J and Loss D 2013 *Phys. Rev. Lett.* **111** 106802
[9] Chang C Z, Zhang J, Feng X, Shen J, Zhang Z, Guo M, Li K, Ou Y, Wei P, Wang L L, Ji Z Q, Feng Y, Ji S, Chen X, Jia J F, Dai X, Fang Z, Zhang S C, He K, Wang Y, Lu L, Ma X C and Xue Q K 2013 *Science* **340** 167
[10] Chen Y L, Chu J H, Analytis J G, Liu Z K, Igarashi K, Kuo H H, Qi X L, Mo S K, Moore R G, Lu D H, Hashimoto M, Sasagawa T, Zhang S C, Fisher I R, Hussain Z and Shen Z X 2010 *Science* **329** 659
[11] Luo W and Qi X L 2013 *Phys. Rev. B* **87** 085431
[12] Qi X L, Li R, Zang J and Zhang S C 2009 *Science* **323** 1184
[13] Li M, Cui W, Yu J, Dai Z, Wang Z, Katmis F, Guo W and Moodera J 2015 *Phys. Rev. B* **91** 014427
[14] Chang C Z, Wei P and Moodera J S 2014 *Mrs Bull.* **39** 867
[15] He K, Ma X C, Chen X, Lu L, Wang Y Y and Xue Q K 2013 *Chin. Phys. B* **22** 067305
[16] Wei P, Katmis F, Assaf B A, Steinberg H, Jarillo-Herrero P, Heiman D and Moodera J S 2013 *Phys. Rev. Lett.* **110** 186807
[17] Katmis F, Lauter V, Nogueira F S, Assaf B A, Jamer M E, Wei P, Satpati B, Freel, J W, Eremin I, Heiman D, Jarillo-Herrero P and Moodera J S 2016 *Nature* **533** 513
[18] Kandala A, Richardella A, Rench D W, Zhang D M, Flanagan T C and Samarth N 2013 *Appl. Phys. Lett.* **103** 202409
[19] Lang M, Montazeri M, Onbasli M C, Kou X, Fan Y, Upadhyaya P, Yao K, Liu F, Jiang Y, Jiang W, Wong K L, Yu G, Tang J, Nie T, He L, Schwartz R N, Wang Y, Ross C A and Wang K L 2014 *Nano Lett.* **14** 3459
[20] Jiang Z, Katmis F, Tang C, Wei P, Moodera J S and Shi J 2014 *Appl. Phys. Lett.* **104** 222409
[21] Jiang Z, Chang C Z, Tang C, Wei P, Moodera J S and Shi J 2015 *Nano Lett.* **15** 5835
[22] Jiang Z, Chang C Z, Tang C, Zheng J G, Moodera J S and Shi J 2016 *AIP Adv.* **6** 055809
[23] Yang W M, Yang S, Zhang Q H, Xu Y, Shen S P, Liao J, Teng J, Nan C W, Gu L, Sun Y, Wu K H and Li Y Q 2014 *Appl. Phys. Lett.* **105** 092411
[24] Zheng G, Wang N, Yang J, Wang W, Du H, Ning W, Yang Z, Lu H Z, Zhang Y and Tian M 2016 *Sci. Rep.* **6** 21334
[25] Tang C, Chang C Z, Zhao G, Liu Y, Jiang Z, Liu C X, McCartney M R, Smith D J, Chen T, Moodera J S and Shi J 2017 *Sci. Adv.* **3** 1700307
[26] Manna P K and Yusuf S M 2014 *Phys. Rep.* **535** 61
[27] Men'shov V N, Tugushev V V, Eremeev S V, Echenique P M and Chulkov E V 2013 *Phys. Rev. B* **88** 224401
[28] Zhang G, Qin H, Teng J, Guo J, Guo Q, Dai X, Fang Z and Wu K 2009 *Appl. Phys. Lett.* **95** 053114
[29] Zhang G, Qin H, Chen J, He X, Lu L, Li Y and Wu K 2011 *Adv. Funct. Mater.* **21** 2351
[30] Richardella A, Zhang D M, Lee J S, Koser A, Rench D W, Yeats A L, Buckley B B, Awschalom D D and Samarth N 2010 *Appl. Phys. Lett.* **97** 262104
[31] Wang Z Y, Li H D, Guo X, Ho W K, Xie M H 2011 *J. Cryst. Growth* **334** 96
[32] Li C H, van't Erve O M J, Robinson J T, Liu Y, Li L and Jonker B T 2014 *Nat. Nanotechnol.* **9** 218
[33] Ginley T P, Wang Y and Law S 2016 *Crystals* **6** 154
[34] Ji H, Stokes R A, Alegria L D, Blomberg E C, Tanatar M A, Reijnders A, Schoop L M, Liang T, Prozorov R, Burch K S, Ong N P, Petta J R and Cava R J 2013 *J. Appl. Phys.* **114** 114907
[35] Meng D, Guo H, Cui Z, Ma C, Zhao J, Lu J, Xu H, Wang Z, Hu X, Fu Z, Peng R, Guo J, Zhai X, Brown G, Knize R and Lu Y 2018 *PNAS* **115** 2873
[36] Fuchs D, Arac E, Pinta C, Schuppler S, Schneider R and Löhneysen H 2008 *Phys. Rev. B* **77** 014434

[37] Rivadulla F, Bi Z, Bauer E, Rivas-Murias B, Vila-Fungueiriño J M and Jia Q 2013 *Chem. Mater.* **25** 55
[38] Freel, J W, Ma J X and Shi J 2008 *Appl. Phys. Lett.* **93** 212501
[39] Zhu S, Meng D, Liang G, Shi G, Zhao P, Cheng P, Li Y, Zhai X, Lu Y, Chen L and Wu K 2018 *Nanoscale* **10** 10041
[40] Zhang Y, He K, Chang C Z, Song C L, Wang L L, Chen X, Jia J F, Fang Z, Dai X, Shan W Y, Shen S Q, Niu Q, Qi X L, Zhang S C, Ma X C and Xue Q K 2010 *Nat. Phys.* **6** 584
[41] Chen J, Qin H J, Yang F, Liu J, Guan T, Qu F M, Zhang G H, Shi J R, Xie X C, Yang C L, Wu K H, Li Y Q and Lu L 2010 *Phys. Rev. Lett.* **105** 176602
[42] Chen J, He X Y, Wu K H, Ji Z Q, Lu L, Shi J R, Smet J H and Li Y Q 2011 *Phys. Rev. B* **83** 241304(R)
[43] Checkelsky J G, Hor Y S, Cava R J and Ong N P 2011 *Phys. Rev. Lett.* **106** 196801
[44] Kim Y S, Brahlek M, Bansal N, Edrey E, Kapilevich G A, Iida K, Tanimura M, Horibe Y, Cheong S W and Oh S 2011 *Phys. Rev. B* **84** 073109
[45] Bansal N, Kim Y S, Brahlek M, Edrey E and Oh S 2012 *Phys. Rev. Lett.* **109** 116804
[46] Lu H Z, Shi J R and Shen S Q 2011 *Phys. Rev. Lett.* **107** 076801
[47] Hikami S, Larkin A I and Nagaoka Y 1980 *Prog. Theor. Phys.* **63** 707
[48] Lin C J, He X Y, Liao J, Wang X X, Sacksteder I V V, Yang W M, Guan T, Zhang Q M, Gu L, Zhang G Y, Zeng C G, Dai X, Wu K H and Li Y Q 2013 *Phys. Rev. B* **88** 041307(R)